Microglial-associated responses to comorbid amyloid pathology and hyperhomocysteinemia in an aged knock-in mouse model of Alzheimer's disease

David James Braun
University of Kentucky https://orcid.org/0000-0002-6967-0489
Edgardo Dimayuga
University of Kentucky Sanders-Brown Center on Aging
Josh M. Morganti
University of Kentucky Sanders-Brown Center on Aging
Linda J Van Eldik (linda.vaneldik@uky.edu)
https://orcid.org/0000-0002-8139-6400

Research

Keywords: Alzheimer's disease, amyloid, homocysteine, hyperhomocysteinemia, microglia, neuroinflammation

Posted Date: February 18th, 2020

DOI: https://doi.org/10.21203/rs.2.23797/v1

Version of Record: A version of this preprint was published on September 17th, 2020. See the published version at https://doi.org/10.1186/s12974-020-01938-7.

Abstract

Background: Elevated blood homocysteine levels, termed hyperhomocysteinemia (HHcy), is a prevalent risk factor for Alzheimer's disease (AD) in elderly populations. While dietary supplementation of B-vitamins is a generally effective method to lower homocysteine levels, there is little if any benefit to cognition. In the context of amyloid pathology, dietary-induced HHcy is known to enhance amyloid deposition and certain inflammatory responses. Little is known, however, about the specific effects on microglia resulting from combined amyloid and HHcy pathologies.

Methods: The present study used a knock-in mouse model of amyloidosis, aged to 12 months, given 8 weeks of dietary deficiency-induced HHcy to better understand how microglia are affected in this comorbidity context.

Results: We found that HHcy-inducing diet increased amyloid plaque burden, altered the neuroinflammatory milieu, and upregulated the expression of multiple damage-associated and "homeostatic" microglial genes.

Conclusions: Taken together, these data indicate complex effects of comorbid pathologies on microglial function that are not driven solely by increased amyloid burden. Given the highly dynamic nature of microglia, their central role in AD pathology, and the frequent occurrence of various comorbidities in AD patients, it is increasingly important to understand how microglia respond to mixed pathological processes.

Background

Homocysteine (Hcy) is an intermediary in essential cellular pathways, and its metabolism depends on several vitamin cofactors, primarily B_6, B_9 (folic acid), and B_{12}. Deficiencies in one or more of these is therefore a common cause of elevated blood homocysteine, termed hyperhomocysteinemia (HHcy).This condition has long been recognized as a vascular risk factor and it has recently garnered considerable attention as a modifiable risk factor for Alzheimer's disease (AD) [1, 2]. The normal human range for Hcy in plasma is generally considered to be less than 15 μM, with increasing levels categorized as moderate (15–30 μM), intermediate (30–100 μM), or severe (> 100 μM) HHcy. Strikingly, the population attributable risk of dementia from raised Hcy is estimated to be between 4 and 31%; in other words, preventing HHcy could prevent somewhere between 1 in 25 to 1 in 3 cases of AD [3]. In the United States alone, even the conservative estimate would translate to hundreds of thousands of people. It follows, then, that reduction of HHcy in the population is an attractive goal. In addition to lifestyle modifications (e.g. quitting smoking, exercise) B-vitamin supplementation is a fairly straightforward intervention that reduces circulating Hcy levels and thus the prevalence of HHcy [4]. Encouragingly, since the United States began supplementing grain with folic acid in the late 1990's, the prevalence of HHcy has roughly halved [5], and this could potentially be a contributor to the recently reported reductions in the rate of increase in AD incidence [6]. Nonetheless, correcting the metabolic dysfunctions underlying elevated Hcy appears to be a

necessary but insufficient step to abrogate the full contribution of this risk factor to AD-associated cognitive decline [3], and adjunct treatments will likely be important moving forward.

HHcy-related neural dysfunction is a multifactorial pathological process, mediated by complex and interacting pathways related to oxidative damage, inflammation, hypomethylation, and others [7]. In this regard it shares commonalities with AD, and there may be important points of convergence amenable to therapeutic targeting. Recent work has highlighted the role of microglia as a nexus in the development and progression of AD pathology (for review see [8]. Microglial responses to pathological Hcy elevation are less well-characterized. However, there is evidence that homocysteine directly increases activation of microglial-type cells in vitro [9, 10], and both direct Hcy supplementation [11] and vitamin deficiency-induced HHcy have similar impacts in vivo [12–14]. Microglial dysregulation could therefore represent one such convergence point in the context of comorbid HHcy and amyloid pathology. The goal of the present study is to better understand this possibility by using a knock-in (KI) mouse model of amyloidosis with dietary-induced HHcy. Mice aged 12 months were placed on B-vitamin deficient diet for 8 weeks and effects on various neuroinflammatory and microglial parameters were characterized. We found that elevation of homocysteine level in the context of amyloid pathology enhances parenchymal plaque deposition, alters the neuroinflammatory milieu, and influences a number of genes important to microglial functioning.

Methods

Animals and experimental design

All mice were housed 1-5 per cage (503.22 usable cm^2) in a room at 23°C ± 2°C, under a 14/10-hour light/dark cycle beginning at 6:00 AM, with *ad libitum* access to water and chow. The $APP^{NLh/NLh}$ x $PS1^{P264L/P264L}$ double knock-in (KI) mouse model expresses humanized amyloid precursor protein with the Swedish mutation (K670N/M671L), along with a P264L point mutation in the mouse presenilin 1 gene [15]. The homozygous KI mice were maintained on a combined CD-1/129 background, with wildtype (WT) controls derived separately from matings of heterozygous KI animals. The experiment was carried out in a 2 x 2 diet by genotype design, where half the mice of each genotype were randomized to receive 8 weeks of control (Envigo, #TD.01636) or HHcy diet (Envigo, #TD.97345), beginning between 52 and 54 weeks of age (M = 53.4 weeks, SD = 0.36). The HHcy diet was deficient in vitamins B6, B9, and B12 and supplemented with excess methionine, while the control diet was nutritionally matched with normal methionine and B vitamin levels [16]. Three mice died during the study and were excluded from all analyses: one KI female receiving HHcy diet, one WT male receiving control diet, and one WT male receiving HHcy diet. The final numbers of mice for each group were 8 WT on control diet (5 female), 10 WT on HHcy diet (5 female), 11 KI on control diet (4 female), and 10 KI on HHcy diet (8 female). The experiment was performed in compliance with the Institutional Animal Care and Use Committee of the University of Kentucky.

Tissue collection and blood analyses

Mice were deeply anesthetized with 5% isoflurane, and arterial blood collected from the left ventricle and placed into EDTA-plasma tubes (Greiner Bio-One, #454428) for separation of plasma by centrifugation (2000xg for 20 minutes at room temperature) followed by storage at -80°C. Plasma samples from a subset of 5 mice per group were diluted 1:5 in ARCHITECT Multi-Assay Manual Diluent (Abbott Laboratories, Chicago, IL, USA) and delivered to the University of Kentucky Clinical Laboratory for Hcy measurement on an ARCHITECT i2000SR analyzer (Abbott Laboratories). An additional subset of 7 WT mice (4 on HHcy and 3 on control diet) had whole blood taken for hematologic analysis using i-STAT CG8+ cartridges (Abbott Laboratories) according to manufacturer's instructions. All mice subsequently underwent transcardial perfusion with 50 ml ice-cold phosphate buffered saline (PBS) at a flow rate of 10 ml/min before decapitation and brain removal and dissection. The right hemisphere was post-fixed in 4% paraformaldehyde for 24 hours at 4°C and cryo-protected in 30% sucrose for at least 48 hours at 4°C. Samples were subsequently cut into 30 mm sections with a sliding microtome and stored in cryoprotectant solution at -20°C prior to immunofluorescent staining. The hippocampus and overlying cortex were dissected from the left hemisphere, flash frozen in liquid nitrogen, and stored at -80°C until processing for biochemical endpoints.

Immunofluorescence

Staining was performed on free-floating sections spaced approximately 300 microns apart through the dorsal hippocampus and overlying cortex, for a total of 6-8 sections per animal. Blocking was performed with 10% normal goat serum (Lampire Biological Laboratories, #7332500) and 0.2% Triton X-100 in PBS. All antibodies were diluted in PBS with 3% normal goat serum and 0.2% Triton X-100. Sections were incubated overnight at 4°C with rabbit anti-P2ry12 (1:500, Anaspec #AS-55043A) and mouse anti-Ab 6E10 conjugated to Alexa 647 (1:200, BioLegend #803021). Samples were subsequently incubated at room temperature for 2 hours in 1:500 secondary antibody solution with Alexa 488 goat anti-rabbit (Invitrogen, #A-11034). Sections were mounted and treated for 5 minutes with 1x TrueBlack (VWR, #10119-144) in 70% ethanol to reduce autofluorescence before drying and coverslipping in Vectashield mounting medium with DAPI (Vector Laboratories, #H-1200). Slides were imaged on a Zeiss Axio Scan Z1 digital slide scanner at 20x magnification.

Image analysis

The dorsal hippocampus and overlying cortex were manually outlined in the HALO analysis suite (Indica Labs, version 2.3.2089.34) by an investigator blinded to experimental groups. The algorithm minimum intensity settings for all analyses were thresholded based upon negative control (no primary antibody) samples. For cortical and hippocampal analyses of P2ry12 staining, and P2ry12 and 6E10 co-

localization, the positive pixel algorithm (Area Quantification FL v1.2) was applied to the traced region across all sections per animal to give a single value of total percent area stained per region per mouse. For cortical and hippocampal analyses of 6E10 staining, the object counter algorithm (Object Colocalization FL v1.0) was applied to the traced region across all sections to give a single average count per square mm of tissue per region. For the spatial analysis of microglia around amyloid plaques, 1-3 individual plaques were manually circled per section within the outlined cortex region, totaling 8-10 plaques per animal. A series of three concentric rings, each 30 microns in width, were drawn around the centered plaque and the positive pixel algorithm was applied within each ring (inner, middle, and outer). Plaques were chosen such that the ring analysis regions were non-overlapping between plaques.

MesoScale Discovery (MSD) multiplex ELISA

Dissected hippocampal and cortical tissue pieces were homogenized using an Omni Bead Ruptor 24 (Omni International) at a 1:20 weight to volume ratio in lysis buffer: PBS with 1 mM PMSF, 0.5 mM EDTA and 0.2X Halt Protease Inhibitor Cocktail (Thermo Scientific, #87786). Homogenates were centrifuged at 12,000xg for 20 minutes at 4°C. Supernatants were collected for cytokine measurement using MSD custom V-Plex ELISA kits according to manufacturer instruction with minor modifications. Briefly, 50 mL of supernatant were loaded per well of MSD plate, and the sample was incubated overnight at 4C in an Eppendorf MixMate at 1000 rpm. Cytokine levels were normalized to the total milligrams (mg) of protein loaded in the sample as determined by BCA Protein Assay (ThermoFisher #23225).

Quantitative reverse-transcriptase polymerase chain reaction (qRT-PCR)

RNA was isolated from whole cortex using the RNeasy Plus Mini Kit (Qiagen, #74136) according to manufacturer's instructions. Tissue was weighed and homogenized in an appropriate volume of buffer, and genomic DNA removed with the gDNA eliminator column. The samples were mixed with 70% ethanol, run through the RNeasy column, washed, and eluted in RNase-free water. Quantity and quality of RNA and 260/280 absorbance ratios were assessed using a NanoDrop spectrophotometer (ThermoFisher Scientific). Reverse transcription was performed with the High Capacity cDNA Reverse Transcription kit (Applied Biosystems, #4368814) according to manufacturer's protocol. Real-time PCR was performed on a ViiA 7 Real-Time PCR System (Applied Biosystems) using individual TaqMan® probes for *P2ry12*, *Clec7a*, and *Itgax* and custom TaqMan®Array Cards (ThermoFisher Scientific, #4342253) with TaqMan Fast Advanced Master Mix (ThermoFisher Scientific, #4444557). See **Table 1** for a complete list of genes and probes included on the array. Established microglial markers affected by amyloid pathology were chosen based on recent studies [17, 18]. Relative gene expression was calculated using the $2^{-\Delta\Delta CT}$ method and log2 normalized. HPRT and 18S were used as housekeeping genes for the individual probes and the custom array, respectively.

Statistical analysis, figure generation, and reporting

Analyses and figure generation were performed with JMP Pro 14 (SAS) and Prism 8.3.0 (GraphPad). Two-way analysis of variance (ANOVA) with Sidak's or Dunnett's post-hoc testing and student's t-tests were performed in Prism as indicated in the figure legends or text. Three group comparisons were made with the gene expression data: WT HHcy versus WT control, KI control vs WT control, and KI HHcy versus KI control. To generate the heatmap, group scores were averaged and transformed into z-scores using JMP, then the variable clustering script was run to group genes by similarity of expression pattern prior to visualization in Prism. Where reported in the text, group means are followed by the standard deviation (SD) in parenthesis.

Results

Eight weeks of B-vitamin deficient and methionine supplemented diet induces HHcy and anemia

To verify success of the dietary intervention, animals were monitored for weight loss (Fig. 1A), final plasma homocysteine concentration (Fig. 1B), and hematological parameters (Fig. 1C and D). As expected, mice on the HHcy diet for 8 weeks lost significant weight compared to mice on control diet, regardless of genotype. For WT mice, those on HHcy diet lost 24% (SD = 11%) of their baseline weight versus a gain of 2% (SD = 7%) for those on control diet. The KI mice on HHcy diet lost an average of 11% (SD = 11%) of their baseline weight, versus a gain of 8% (SD = 5%) for those on control diet. The weight loss of WT mice on HHcy diet was significantly greater than that of the KI mice on HHcy diet ($p = 0.0118$, two-way ANOVA with Sidak's post-hoc testing). Despite differences in weight loss, the average plasma homocysteine levels were similar between genotypes, with WT mice achieving an average concentration of 19.0 μM (SD = 6.8 μM) versus 14.7 μM (SD = 2.8 μM) in the KI animals. Values for both genotypes on control diet were below the limit of detection for the test (5 μM) and are not shown. Additionally, whole-blood analysis of a subset of WT mice showed reduced hemoglobin and hematocrit after 8 weeks of HHcy diet, indicative of anemic changes which are another known consequence of B vitamin deficiency [19].

HHcy increases amyloid plaque burden and alters neuroinflammatory markers in KI mice

To determine effects on amyloid deposition, Aβ positive objects (colored white) were counted in dorsal hippocampus and overlying cortex using HALO software (Fig. 2A). HHcy diet induced a significant increase in amyloid plaques (Fig. 2B). In the cortex, average plaque number increased from 13.3 per mm^2 (SD = 6.1) in KI mice on control diet to 29.4 mm^2 (SD = 17.3) in those on HHcy diet. Hippocampal plaques increased from 3.9 (SD = 3.3) to 10.1 (SD = 8.7) per mm^2 in mice on control or HHcy diet, respectively. Notably, no evidence of cerebral amyloid angiopathy (CAA) was found.

To assess whether the increased amyloid plaque burden after HHcy diet exacerbated pro-inflammatory responses, we measured levels of the inflammation-associated molecules CXCL1, CCL3, IL-33, TNFα, IL-6, and IL-1β by multiplexed MSD ELISA. As shown in Fig. 3A, IL-1β levels in cortex are significantly higher in the KI mice compared to the WT mice, but there is no significant additional effect of HHcy diet compared to control diet. In contrast, IL-1β levels are significantly increased by HHcy diet in the hippocampus of KI mice but not WT mice. As shown in Fig. 3B, CCL3 levels are significantly reduced in KI mice compared to WT mice on control diet. CCL3 is significantly reduced in WT animals on HHcy versus control diet, but there is no further decrease in CCL3 in the KI mice on HHcy diet compared to control diet. No significant differences were detected in levels of CXCL1, IL-33, TNFα, or IL-6 in either region or as a function of genotype or diet (data not shown).

To measure microgliosis without inadvertent inclusion of infiltrating myeloid cells, we measured P2ry12 staining as a microglia-specific marker [20] (Fig. 4). There was a significant main effect of genotype on P2ry12 expression in the cortex ($F(1, 29) = 9.973$, $p = 0.0037$), but no differences found in the hippocampus. When groups were compared individually, the only significant difference was an increase in cortical P2ry12 staining in KI versus WT mice on control diet (Fig. 4B). Indeed, there was a modest decrease in P2ry12 staining in the cortex of KI mice on HHcy versus control diet. Because its expression is reportedly downregulated in plaque-associated microglia [18, 21], this finding might be attributable to either additive effects of comorbid amyloid and HHcy pathology, or simply to the increase in plaque burden. To further clarify these possibilities, we next measured parameters relating to microglial migration and P2ry12 expression near amyloid plaques.

HHcy diet does not alter microglial migration to plaques, nor plaque-associated P2ry12 downregulation in KI mice

The percent area double-positive for P2ry12 and Aβ 6E10 staining was unaltered within cortex between KI control (M = .018%, SD = .015) and KI HHcy mice (M = .018%, .012) ($t(18) = 0.0897$, $p = 0.9295$). This was similarly true in the hippocampus of the KI control (M = .013%, SD = .009) and HHcy mice (M = .014%, SD = .011) ($t(18) = 0.1474$, $p = 0.8843$). To more closely examine this relationship, a spatial analysis was performed around a subset of plaques in the cortex to quantify the distribution of microglia within different distances from the plaque (Fig. 5). Results of this analysis were consistent with the previous data indicating a lack of a dietary effect. Specifically, the percent positive area of P2ry12 staining (Fig. 5B) and average pixel intensity (Fig. 5C) were unchanged between dietary groups regardless of proximity to the plaque. The analysis did reveal a relative dearth of P2ry12 staining and a decrease in its

intensity in the inner ring closest to the plaque, in accordance with previous reports of P2ry12 down-regulation near plaques [18, 21]. These data indicate the decline in cortical P2ry12 staining may therefore be primarily attributable to an increase in overall plaque burden rather than a reduction in microgliosis per se, and indicative of a shift in microglial phenotype. To begin exploring this phenotypic change in the comorbid model, we next measured gene expression changes across a panel of 50 genes from whole-tissue cortical samples (Table 1).

HHcy modifies microglial gene expression in WT and KI mice

A subset of 8 mice per group were used for gene expression analysis, with data normalized to the expression level of WT mice (Fig. 6). Some genes were found to be elevated by the diet alone in WT mice (Clec7a, Itgax, Cst7, Tpt1), and some were altered in response to amyloidosis alone (Itgax, Cst7, Fcrls, Golm1, P2ry12, Csf1r). In addition, several genes were differentially regulated in KI HHcy mice versus the KI controls: C1qb, C1qc, Csf1r, Sall1, Lag3, Lyz2, and Clec7a. Interestingly, not only the putative damage-associated genes (Lag3, Clec7a, Lyz2) but also the putative homeostatic markers (C1qb, C1qc, Sall1, Csf1r) were upregulated in the comorbid condition. These findings indicate that comorbid pathologies can have complex and interactive effects on microglial phenotypes in addition to straightforwardly additive ones.

Discussion

We report here several major findings that increase understanding of microglial responses in the context of comorbid amyloid and HHcy-associated pathology. First, 8-weeks of HHcy-inducing diet is sufficient to produce a large increase in parenchymal plaque deposition without overtly altering microgliosis or generating a large response in canonical pro-inflammatory factors. Second, there appears to be no effect on movement of microglia to plaques, nor alteration in their downregulation of the P2ry12 receptor in this context. Third, there were interactive and complex effects of the combined amyloid and HHcy pathologies on microglial gene expression. Together, these findings demonstrate the complexity of microglial responses to perturbations in brain homeostasis and provide the foundation for a more complete characterization of these changes in future studies.

Different methods of HHcy-induction in various mouse models of AD have been shown to modify amyloid burden in parenchyma and vasculature [13, 22–24]. This is reflective of what occurs in patient populations, where plasma Aβ positively correlates with homocysteine levels and elevated Hcy is also associated with higher brain Aβ accumulation and CAA pathology [25–28]. Our results regarding enhanced plaque deposition in hippocampus and cortex are therefore consistent with the literature. Despite the large increase in plaque burden, however, we found fairly modest changes in neuroinflammatory cytokines and chemokines. Of the pro-inflammatory factors measured, only IL-1β was significantly upregulated in the KI mice in response to HHcy, and even this was observed only in the hippocampus. Furthermore, CCL3 was downregulated by HHcy diet in the WT mice but unaffected in the

KI. In fact, baseline CCL3 levels were reduced in KI versus WT mice, contrary to what has been observed in other studies [29, 30]. The significance of this finding is currently unclear, as the general consensus in the literature is that CCL3 is upregulated by amyloid pathology and this is a detrimental change [31, 32]. It is worth noting, however, that at least one study has observed an increase in plaque-associated dystrophic neurites in association with reduced CCL3 [33] which suggests that its upregulation can in some cases be protective, although this may be a correlative rather than causative effect. In any event, the cytokine data herein are in contrast to previous studies that have reported a robust pro-inflammatory response to this diet in either WT or AD model mice [12–14, 22]. Notably, the increase in plasma Hcy level was comparatively less severe in the present study, and the discrepancy may indicate that the pro-inflammatory response is graded depending upon the severity of induced HHcy. The implication of this scenario is that patients with severe HHcy may require treatments suppressing neuroinflammation; those with moderate HHcy may benefit more from alternative approaches. Such possibilities warrant more complete characterization of changes to the neuroinflammatory milieu occurring at different levels of Hcy elevation.

Although a dramatic neuroinflammatory response was not observed in this model, there were several interesting and important findings with regard to microglia. When P2ry12 staining was taken as a marker of microgliosis, we observed the expected increase in staining within the cortex of KI versus WT mice. Interestingly, there was a moderate decrease in P2ry12 in the KI mice on HHcy diet relative to those on control, but no such effect in the WT animals. Given recent findings that microglia downregulate P2ry12 in the presence of amyloid [18, 21], this is consistent with the observed enhancement of amyloid burden. Further, recent research indicates that the P2ry12 receptor is crucial for microglial monitoring of neuronal functioning and the induction of neuroprotective responses [34]. Whether this further reduction in cortical P2ry12 signaling in our comorbidity model might also enhance neuronal dysfunction is currently unknown; however, given reported additive effects on cognitive impairment caused by the presence of amyloid and HHcy pathologies [13, 22], this seems likely.

Results of gene expression profiling indicate an alteration in microglial phenotype that is not strictly attributable to enhanced amyloid deposition. Fifty genes were selected for characterization, chosen based upon recently published datasets [17, 18]. Half of the selected markers are positively regulated by amyloid pathology and considered to be damage- or neurodegeneration-associated markers. The other half are negatively regulated by amyloid pathology and considered as homeostatic markers. Were the microglia simply responding to enhanced plaque burden, then the prediction would be further elevation of damage markers and further suppression of homeostatic genes. While several damage markers were further upregulated by the comorbid pathologies, several homeostatic genes were upregulated as well: C1qb, C1qc, Sall1, and Csf1r. Interestingly, the first two of these encode parts of complement component 1q (C1q), which plays a critical role in synaptic pruning during development and in pathological conditions such as AD [35]. Whether this upregulation translates to enhanced synaptic loss remains to be determined, but it would be consistent with the additive detrimental effects of amyloid and HHcy on cognitive function. Sall1 is a transcription factor that under physiological conditions inhibits microglial activation and pro-inflammatory responses [36]. Its upregulation in this context suggests an impairment

in microglial reactivity to amyloid, and this may help to explain the modest effects on the pro-inflammatory cytokines measured. Additionally, this potential failure of appropriate microglial activation in the presence of amyloid might contribute to the enhanced plaque burden. Csf1r signaling is well-characterized for its involvement in microglial proliferation and survival [37]. Recent studies have shown that chronic pharmacologic suppression of this receptor result in loss of microglia concomitant with protection against neurodegenerative changes in the 5xFAD amyloidosis model [38, 39]. Taken together, these data indicate potentially maladaptive microglial responses to Aβ in the context of HHcy.

Clec7a, Lag3, and Lyz2 were the damage-associated markers found upregulated in the KI mice on HHcy versus control diet. Clec7a is a pathogen-associated molecular pattern receptor involved in the innate immune response, including microglial phagocytic responses [40], and it has been shown to increase in parallel with plaque burden in mouse models of AD [41]. This upregulation may therefore be reflective of the increased Aβ plaque burden in the comorbidity model. Notably, it was also significantly upregulated by HHcy alone. Whether this is due to the presence of elevated homocysteine, anemia or B-vitamin deficiencies, or some combination is currently unknown but should be directly determined in future studies. Little is known regarding the function of Lag3 in the brain. In one study of its role during prion disease, its increase in response to infection was consistent with a function in immune response. In the same study, however, genetic deletion of Lag3 did not alter prion load, inflammatory gene expression, nor neurodegenerative course [42]. In a Parkinson's disease model it mediates the internalization and neuronal propagation of fibrillar alpha-synuclein and its genetic deletion provides benefit, but it does not bind fibrillar Aβ at least in vitro [43]. Its function in the context of amyloid deposition or HHcy is therefore currently unknown. Lyz2 encodes a lysozyme that is increased in response to increased amyloid burden, and its over-expression reduces amyloid-associated toxicity in a drosophila model of AD [44]. While this suggests it may play a protective role in the comorbidity model, it is unclear why it was not upregulated in the KI mice on control diet versus WT. It is worth noting here that Lyz2 is also present in neurons [45], as is Lag3 [43], and several other genes included in this panel are not entirely microglia-specific. As such, the gene expression data as a whole must be interpreted with caution. Indeed, the genes for the panel were chosen based on characterization of a transcriptional program identified in analyses of isolated microglia [17, 18]. That more genes were not detected as being significantly upregulated in our panel is likely due in part to loss of a microglia-specific signature. Alternatively, some of these genes may already be maximally perturbed or simply not responsive to the types of pathology associated with HHcy. Future studies utilizing cellular isolation techniques, combined with unbiased measurement of whole-transcriptome changes will be useful in clarifying microglia-specific alterations in this model. Ultimately, any findings in this and similar mouse models must also be compared to samples from relevant patient populations.

Conclusion

Modulation of microglial function represents a promising area for therapeutic development in Alzheimer's disease research. Given the frequent co-occurrence of multiple pathologies in patients with dementia, the success of this approach will likely require a deeper understanding of microglial responses in various

contexts. The present study supports such efforts by offering a preliminary characterization of unique microglial-associated changes in response to comorbid amyloidosis and HHcy.

Abbreviations

Ab	amyloid beta
AD	Alzheimer's disease
ANOVA	analysis of variance
C1q	complement component 1q
CAA	cerebral amyloid angiopathy
Hcy	homocysteine
HHcy	hyperhomocysteinemia
KI	knock-in
MSD	MesoScale Discovery
PBS	phosphate-buffered saline
qRT-PCR	quantitative reverse-transcriptase polymerase chain reaction
SD	standard deviation
WT	Wildtype

Declarations

Ethics approval

All animal procedures for this study were approved by the Institutional Animal Care and Use Committee of the University of Kentucky.

Consent for publication

Not applicable.

Availability of data and materials

The datasets generated and analyzed for this study are available from the corresponding author upon reasonable request.

Competing interests

The authors declare that they have no competing interests.

Funding

This study was supported by National Institute on Aging Fellowship F32AG058456 (DJB) and National Institute on Aging Grant RF1AG064859 (LVE).

Authors' contributions

DJB and LJVE designed research studies. DJB performed the experiment, harvested the tissue, performed qRT-PCR and tissue staining, analyzed the data, and wrote the manuscript. ED sectioned tissue and performed MSD ELISAs. JMM assisted with experimental design and data analysis. All authors read and approved the final manuscript.

Acknowledgements

We thank Amy Gorman, Danielle Goulding, and Alex Early for their technical assistance with this project.

References

1. Price BR, Wilcock DM, Weekman EM: Hyperhomocysteinemia as a Risk Factor for Vascular Contributions to Cognitive Impairment and Dementia. *Front Aging Neurosci* 2018, 10:350.
2. Selhub J: Homocysteine metabolism. *Annu Rev Nutr* 1999, 19:217-246.
3. Smith AD, Refsum H, Bottiglieri T, Fenech M, Hooshmand B, McCaddon A, Miller JW, Rosenberg IH, Obeid R: Homocysteine and Dementia: An International Consensus Statement. *J Alzheimers Dis* 2018, 62(2):561-570.

4. Clarke R, Halsey J, Lewington S, Lonn E, Armitage J, Manson JE, Bonaa KH, Spence JD, Nygard O, Jamison R *et al*: Effects of lowering homocysteine levels with B vitamins on cardiovascular disease, cancer, and cause-specific mortality: Meta-analysis of 8 randomized trials involving 37 485 individuals. *Arch Intern Med* 2010, 170(18):1622-1631.
5. Jacques PF, Selhub J, Bostom AG, Wilson PW, Rosenberg IH: The effect of folic acid fortification on plasma folate and total homocysteine concentrations. *N Engl J Med* 1999, 340(19):1449-1454.
6. Langa KM, Larson EB, Crimmins EM, Faul JD, Levine DA, Kabeto MU, Weir DR: A Comparison of the Prevalence of Dementia in the United States in 2000 and 2012. *JAMA Intern Med* 2017, 177(1):51-58.
7. Obeid R, Herrmann W: Mechanisms of homocysteine neurotoxicity in neurodegenerative diseases with special reference to dementia. *FEBS Lett* 2006, 580(13):2994-3005.
8. Hemonnot AL, Hua J, Ulmann L, Hirbec H: Microglia in Alzheimer Disease: Well-Known Targets and New Opportunities. *Front Aging Neurosci* 2019, 11:233.
9. Wan L, Sun Y, Zhang F, Ren Y: Low-Dose Homocystine Enhances Proliferation and Migration of Bv2 Microglia Cells. *Cell Mol Neurobiol* 2016, 36(8):1279-1289.
10. Weekman EM, Woolums AE, Sudduth TL, Wilcock DM: Hyperhomocysteinemia-Induced Gene Expression Changes in the Cell Types of the Brain. *ASN Neuro* 2017, 9(6):1759091417742296.
11. Chen S, Dong Z, Cheng M, Zhao Y, Wang M, Sai N, Wang X, Liu H, Huang G, Zhang X: Homocysteine exaggerates microglia activation and neuroinflammation through microglia localized STAT3 overactivation following ischemic stroke. *J Neuroinflammation* 2017, 14(1):187.
12. Sudduth TL, Powell DK, Smith CD, Greenstein A, Wilcock DM: Induction of hyperhomocysteinemia models vascular dementia by induction of cerebral microhemorrhages and neuroinflammation. *J Cereb Blood Flow Metab* 2013, 33(5):708-715.
13. Sudduth TL, Weekman EM, Brothers HM, Braun K, Wilcock DM: beta-amyloid deposition is shifted to the vasculature and memory impairment is exacerbated when hyperhomocysteinemia is induced in APP/PS1 transgenic mice. *Alzheimers Res Ther* 2014, 6(3):32.
14. Sudduth TL, Weekman EM, Price BR, Gooch JL, Woolums A, Norris CM, Wilcock DM: Time-course of glial changes in the hyperhomocysteinemia model of vascular cognitive impairment and dementia (VCID). *Neuroscience* 2017, 341:42-51.
15. Flood DG, Reaume AG, Dorfman KS, Lin YG, Lang DM, Trusko SP, Savage MJ, Annaert WG, De Strooper B, Siman R *et al*: FAD mutant PS-1 gene-targeted mice: increased A beta 42 and A beta deposition without APP overproduction. *Neurobiol Aging* 2002, 23(3):335-348.
16. Braun DJ, Abner E, Bakshi V, Goulding DS, Grau EM, Lin AL, Norris CM, Sudduth TL, Webster SJ, Wilcock DM *et al*: Blood Flow Deficits and Cerebrovascular Changes in a Dietary Model of Hyperhomocysteinemia. *ASN Neuro* 2019, 11:1759091419865788.
17. Keren-Shaul H, Spinrad A, Weiner A, Matcovitch-Natan O, Dvir-Szternfeld R, Ulland TK, David E, Baruch K, Lara-Astaiso D, Toth B *et al*: A Unique Microglia Type Associated with Restricting Development of Alzheimer's Disease. *Cell* 2017, 169(7):1276-1290 e1217.

18. Krasemann S, Madore C, Cialic R, Baufeld C, Calcagno N, El Fatimy R, Beckers L, O'Loughlin E, Xu Y, Fanek Z *et al*: The TREM2-APOE Pathway Drives the Transcriptional Phenotype of Dysfunctional Microglia in Neurodegenerative Diseases. *Immunity* 2017, 47(3):566-581 e569.
19. Bianchi VE: Role of nutrition on anemia in elderly. *Clin Nutr ESPEN* 2016, 11:e1-e11.
20. Butovsky O, Jedrychowski MP, Moore CS, Cialic R, Lanser AJ, Gabriely G, Koeglsperger T, Dake B, Wu PM, Doykan CE *et al*: Identification of a unique TGF-beta-dependent molecular and functional signature in microglia. *Nat Neurosci* 2014, 17(1):131-143.
21. Jay TR, Miller CM, Cheng PJ, Graham LC, Bemiller S, Broihier ML, Xu G, Margevicius D, Karlo JC, Sousa GL *et al*: TREM2 deficiency eliminates TREM2+ inflammatory macrophages and ameliorates pathology in Alzheimer's disease mouse models. *J Exp Med* 2015, 212(3):287-295.
22. Weekman EM, Sudduth TL, Price BR, Woolums AE, Hawthorne D, Seaks CE, Wilcock DM: Time course of neuropathological events in hyperhomocysteinemic amyloid depositing mice reveals early neuroinflammatory changes that precede amyloid changes and cerebrovascular events. *J Neuroinflammation* 2019, 16(1):284.
23. Li JG, Pratico D: High levels of homocysteine results in cerebral amyloid angiopathy in mice. *J Alzheimers Dis* 2015, 43(1):29-35.
24. Li JG, Barrero C, Merali S, Pratico D: Five lipoxygenase hypomethylation mediates the homocysteine effect on Alzheimer's phenotype. *Sci Rep* 2017, 7:46002.
25. Luchsinger JA, Tang MX, Miller J, Green R, Mehta PD, Mayeux R: Relation of plasma homocysteine to plasma amyloid beta levels. *Neurochem Res* 2007, 32(4-5):775-781.
26. Irizarry MC, Gurol ME, Raju S, Diaz-Arrastia R, Locascio JJ, Tennis M, Hyman BT, Growdon JH, Greenberg SM, Bottiglieri T: Association of homocysteine with plasma amyloid beta protein in aging and neurodegenerative disease. *Neurology* 2005, 65(9):1402-1408.
27. Hooshmand B, Polvikoski T, Kivipelto M, Tanskanen M, Myllykangas L, Erkinjuntti T, Makela M, Oinas M, Paetau A, Scheltens P *et al*: Plasma homocysteine, Alzheimer and cerebrovascular pathology: a population-based autopsy study. *Brain* 2013, 136(Pt 9):2707-2716.
28. Chung YC, Kruyer A, Yao Y, Feierman E, Richards A, Strickland S, Norris EH: Hyperhomocysteinemia exacerbates Alzheimer's disease pathology by way of the beta-amyloid fibrinogen interaction. *J Thromb Haemost* 2016, 14(7):1442-1452.
29. Tripathy D, Thirumangalakudi L, Grammas P: Expression of macrophage inflammatory protein 1-alpha is elevated in Alzheimer's vessels and is regulated by oxidative stress. *J Alzheimers Dis* 2007, 11(4):447-455.
30. Kang SS, Ebbert MTW, Baker KE, Cook C, Wang X, Sens JP, Kocher JP, Petrucelli L, Fryer JD: Microglial translational profiling reveals a convergent APOE pathway from aging, amyloid, and tau. *J Exp Med* 2018, 215(9):2235-2245.
31. Passos GF, Figueiredo CP, Prediger RD, Pandolfo P, Duarte FS, Medeiros R, Calixto JB: Role of the macrophage inflammatory protein-1alpha/CC chemokine receptor 5 signaling pathway in the

neuroinflammatory response and cognitive deficits induced by beta-amyloid peptide. *Am J Pathol* 2009, 175(4):1586-1597.

32. Marciniak E, Faivre E, Dutar P, Alves Pires C, Demeyer D, Caillierez R, Laloux C, Buee L, Blum D, Humez S: The Chemokine MIP-1alpha/CCL3 impairs mouse hippocampal synaptic transmission, plasticity and memory. *Sci Rep* 2015, 5:15862.
33. Ulrich JD, Ulland TK, Mahan TE, Nystrom S, Nilsson KP, Song WM, Zhou Y, Reinartz M, Choi S, Jiang H *et al*: ApoE facilitates the microglial response to amyloid plaque pathology. *J Exp Med* 2018, 215(4):1047-1058.
34. Cserep C, Posfai B, Lenart N, Fekete R, Laszlo ZI, Lele Z, Orsolits B, Molnar G, Heindl S, Schwarcz AD *et al*: Microglia monitor and protect neuronal function via specialized somatic purinergic junctions. *Science* 2019.
35. Rajendran L, Paolicelli RC: Microglia-Mediated Synapse Loss in Alzheimer's Disease. *J Neurosci* 2018, 38(12):2911-2919.
36. Buttgereit A, Lelios I, Yu X, Vrohlings M, Krakoski NR, Gautier EL, Nishinakamura R, Becher B, Greter M: Sall1 is a transcriptional regulator defining microglia identity and function. *Nat Immunol* 2016, 17(12):1397-1406.
37. Chitu V, Gokhan S, Nandi S, Mehler MF, Stanley ER: Emerging Roles for CSF-1 Receptor and its Ligands in the Nervous System. *Trends Neurosci* 2016, 39(6):378-393.
38. Sosna J, Philipp S, Albay R, 3rd, Reyes-Ruiz JM, Baglietto-Vargas D, LaFerla FM, Glabe CG: Early long-term administration of the CSF1R inhibitor PLX3397 ablates microglia and reduces accumulation of intraneuronal amyloid, neuritic plaque deposition and pre-fibrillar oligomers in 5XFAD mouse model of Alzheimer's disease. *Mol Neurodegener* 2018, 13(1):11.
39. Spangenberg E, Severson PL, Hohsfield LA, Crapser J, Zhang J, Burton EA, Zhang Y, Spevak W, Lin J, Phan NY *et al*: Sustained microglial depletion with CSF1R inhibitor impairs parenchymal plaque development in an Alzheimer's disease model. *Nat Commun* 2019, 10(1):3758.
40. Shah VB, Huang Y, Keshwara R, Ozment-Skelton T, Williams DL, Keshvara L: Beta-glucan activates microglia without inducing cytokine production in Dectin-1-dependent manner. *J Immunol* 2008, 180(5):2777-2785.
41. Kamphuis W, Kooijman L, Schetters S, Orre M, Hol EM: Transcriptional profiling of CD11c-positive microglia accumulating around amyloid plaques in a mouse model for Alzheimer's disease. *Biochim Biophys Acta* 2016, 1862(10):1847-1860.
42. Liu Y, Sorce S, Nuvolone M, Domange J, Aguzzi A: Lymphocyte activation gene 3 (Lag3) expression is increased in prion infections but does not modify disease progression. *Sci Rep* 2018, 8(1):14600.
43. Mao X, Ou MT, Karuppagounder SS, Kam TI, Yin X, Xiong Y, Ge P, Umanah GE, Brahmachari S, Shin JH *et al*: Pathological alpha-synuclein transmission initiated by binding lymphocyte-activation gene 3. *Science* 2016, 353(6307).
44. Sandin L, Bergkvist L, Nath S, Kielkopf C, Janefjord C, Helmfors L, Zetterberg H, Blennow K, Li H, Nilsberth C *et al*: Beneficial effects of increased lysozyme levels in Alzheimer's disease modelled in

Drosophila melanogaster. *FEBS J* 2016, 283(19):3508-3522.

45. Orthgiess J, Gericke M, Immig K, Schulz A, Hirrlinger J, Bechmann I, Eilers J: Neurons exhibit Lyz2 promoter activity in vivo: Implications for using LysM-Cre mice in myeloid cell research. *Eur J Immunol* 2016, 46(6):1529-1532.

Tables

Gene	TaqMan probe	Gene	TaqMan Probe
Apoe	Mm01307193_g1	Ftl1	Mm03030144_g1
B2m	Mm00437762_m1	Fth1	Mm00850707_g1
C1qa	Mm00432142_m1	Golm1	Mm00550918_m1
C1qb	Mm01179619_m1	Gpr34	Mm02620221_s1
C1qc	Mm00776126_m1	Hexb	Mm01282432_m1
Ccl2	Mm00441242_m1	Hif1a	Mm00468869_m1
Ccrl2	Mm00516914_g1	Kctd12	Mm00624816_s1
Cd74	Mm00658576_m1	Lag3	Mm00493071_m1
Chil3	Mm00657889_mH	Lyz2	Mm01612741_m1
Csf1	Mm00432686_m1	Mafb	Mm00627481_s1
Csf1r	Mm01266652_m1	Olfml3	Mm00513567_m1
Cst3	Mm00438347_m1	Pde3b	Mm00691635_m1
Cst7	Mm00438351_m1	Plxdc2	Mm00470653_m1
Ctsz	Mm00517697_m1	Sall1	Mm00491266_m1
Ctsb	Mm01310506_m1	Slc11a1	Mm00443045_m1
Ctsd	Mm00515586_m1	Slco2b1	Mm00614448_m1
Ctsl	Mm00515597_m1	Spp1	Mm00436767_m1
Ctss	Mm01255859_m1	Tgfbr1	Mm00436964_m1
Axl	Mm00437221_m1	Tpt1	Mm03009502_g1
Cx3cr1	Mm02620111_s1	Tyrobp	Mm00449152_m1
Cyba	Mm00514478_m1	Mertk	Mm00434920_m1
Eef1a1	Mm01973893_g1	18S	Hs99999901_s1
Egr1	Mm00656724_m1	**Clec7a**	**Mm01183349_m1**
P2ry13	Mm01951265_s1	**P2ry12**	**Mm00446026_m1**
F11r	Mm00554113_m1	**Itgax**	**Mm00498701_m1**
Fcrls	Mm00472833_m1	**Hprt**	**Mm00446968_m1**

Table 1: Gene names and TaqMan probes analyzed in this study. Genes in bold were run with individual probes: the rest were run together on TaqMan custom low-density array cards.

Figures

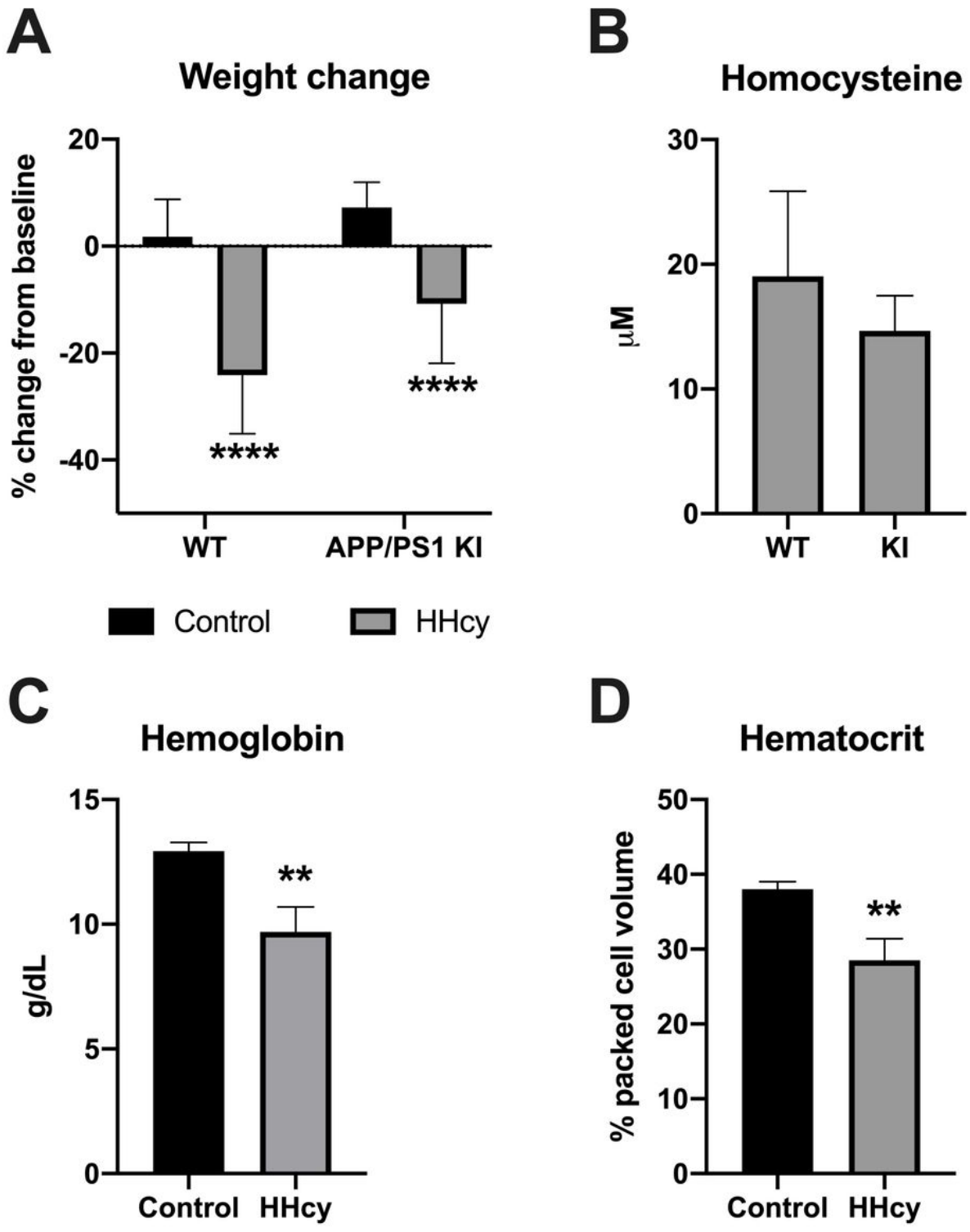

Figure 1

Validation of dietary HHcy model. Both genotypes lost significant weight on HHcy versus control diet, although WT mice lost more (A). Despite differences in endpoint weight loss, eight weeks of HHcy diet resulted in similar plasma homocysteine elevation in both WT and KI mice, n = 5 per group (B). A subset

of WT mice had blood taken to measure hemoglobin (C) and hematocrit level (D) and HHcy diet was found to significantly reduce both. ****p < .001 versus within genotype control, two-way ANOVA with Sidak's post-hoc tests. **p < .01 versus control diet, student's t-test.

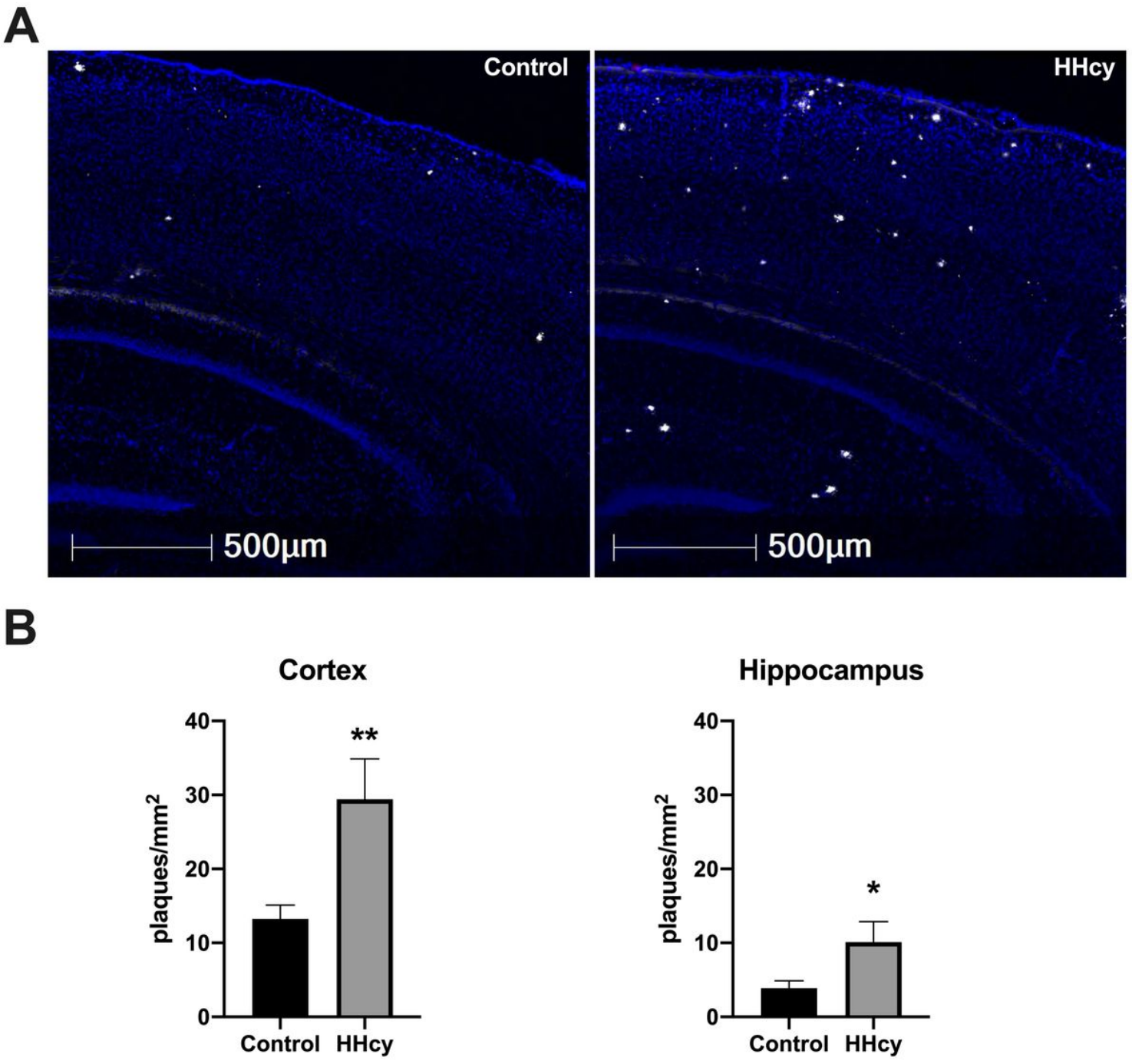

Figure 2

Effect of dietary HHcy on amyloid plaque production in KI mice. (A) Representative images of the dorsal hippocampus and overlying cortex from KI mice on control diet (left panel) or HHcy diet (right panel). Visualization of nuclei with DAPI is colored blue, A 6E10 positivity is colored white. (B) Quantification of average plaques per square mm in the cortex (left panel) and hippocampus (right panel), n =11 control

and 10 HHcy KI mice. Black bars indicate control diet, gray bars indicate HHcy diet. **p < .01, *p < .05 versus control, student's t-test.

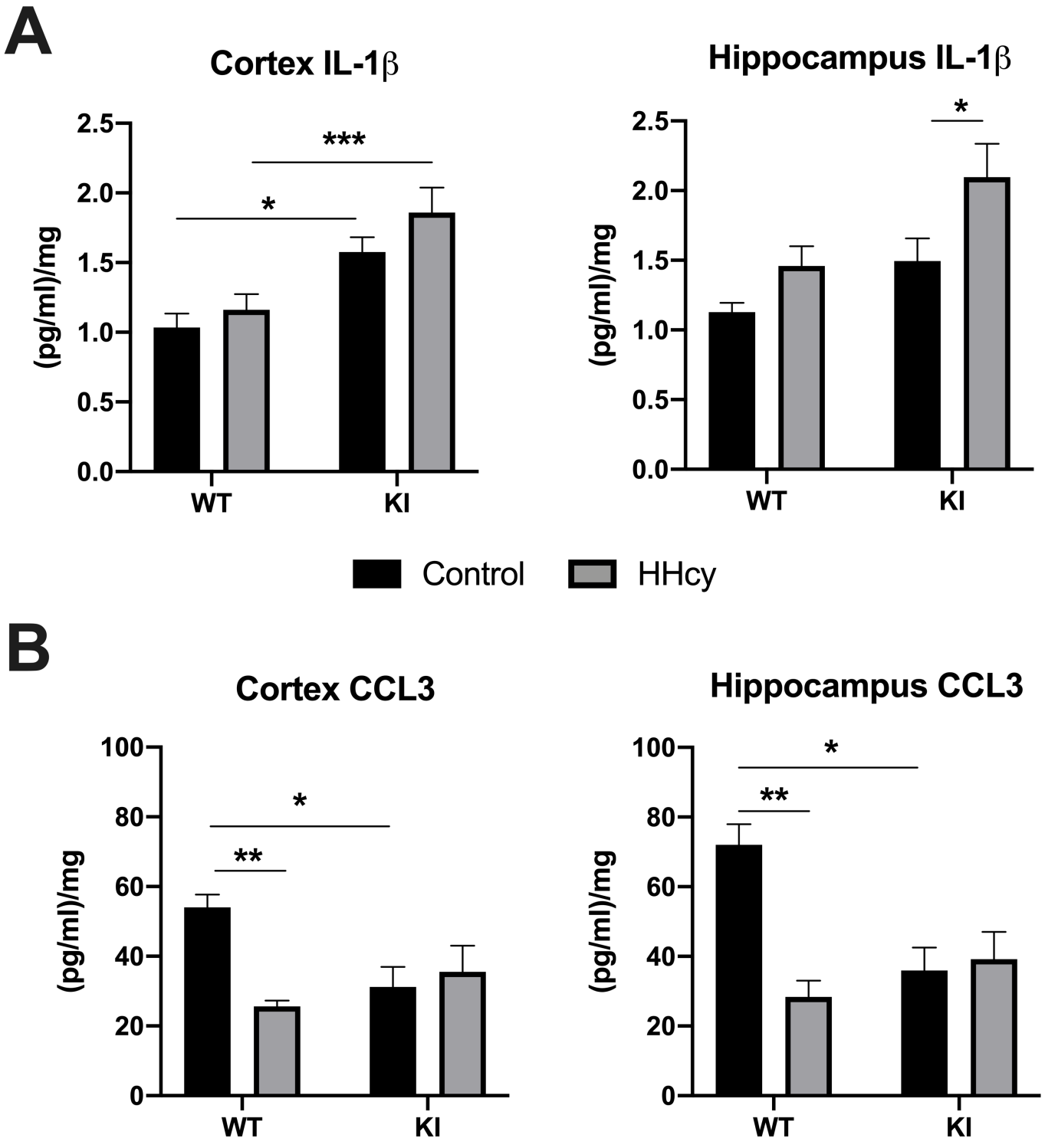

Figure 3

Effect of HHcy on cytokines. Effect of HHcy on cortical and hippocampal levels of (A) IL-1β and (B) CCL3 are shown. IL-1β levels in cortex are higher in KI mice compared to WT mice, but there is no additional effect of HHcy diet in this region. In contrast, IL-1β levels are significantly increased by HHcy diet in the

hippocampus of KI mice but not WT mice. In both cortex and hippocampus, CCL3 levels are significantly reduced in KI mice compared to WT mice on control diet. CCL3 is significantly reduced in WT but not KI mice on the HHcy versus control diet, but there is no further decrease in CCL3 in KI mice on HHcy diet compared to control. *p < .05, **p < .01, ***p < .005 versus indicated group, two-way ANOVA with Sidak's post-hoc tests, n = 8-11 per group.

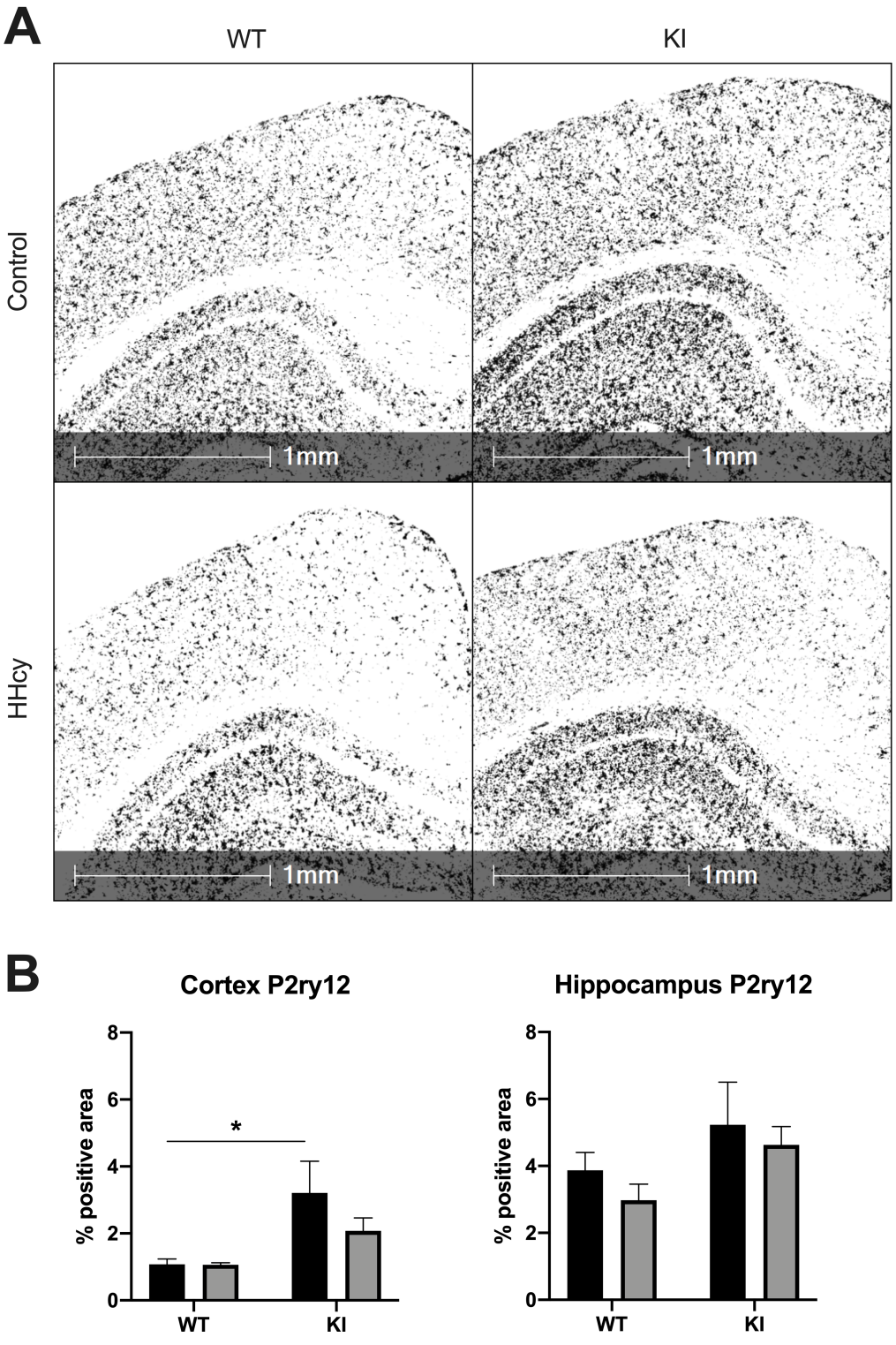

Figure 4

P2ry12 staining in the hippocampus and overlying cortex. Representative images of the analyzed regions are shown in (A), where P2ry12 staining is shown in black. Total % positive area is quantified for the cortex and hippocampus in (B). *p < .05 versus WT control mice, two-way ANOVA with Sidak's post-hoc tests, n = 7-10 per group

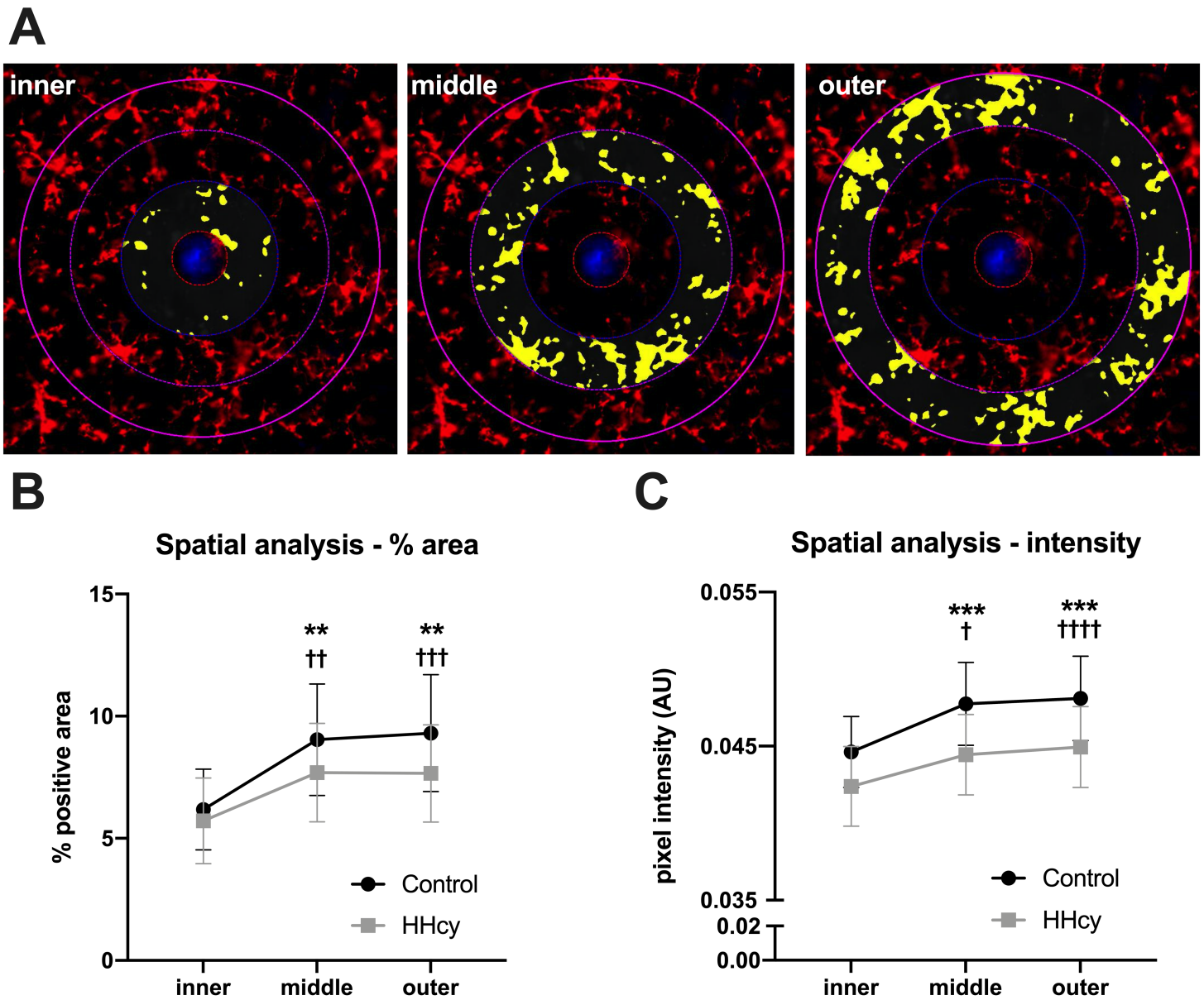

Figure 5

Spatial analysis of P2ry12 positive microglia near plaques in KI. Representative images of analysis regions are shown in (A) where P2ry12 staining is in red, 6E10 staining is in blue, and output of the analysis algorithm is shown in yellow. Total % positive area for P2ry12 is quantified in (B), and average pixel intensity within each region shown in (C). **p < .01, ***p < .005 versus the inner ring within KI mice on control diet, mixed measures two-way ANOVA with Dunnett's post-hoc tests. †p < .05, ††p < .005, †††p < .001, ††††p < .0001 versus the inner ring within KI mice on HHcy diet.

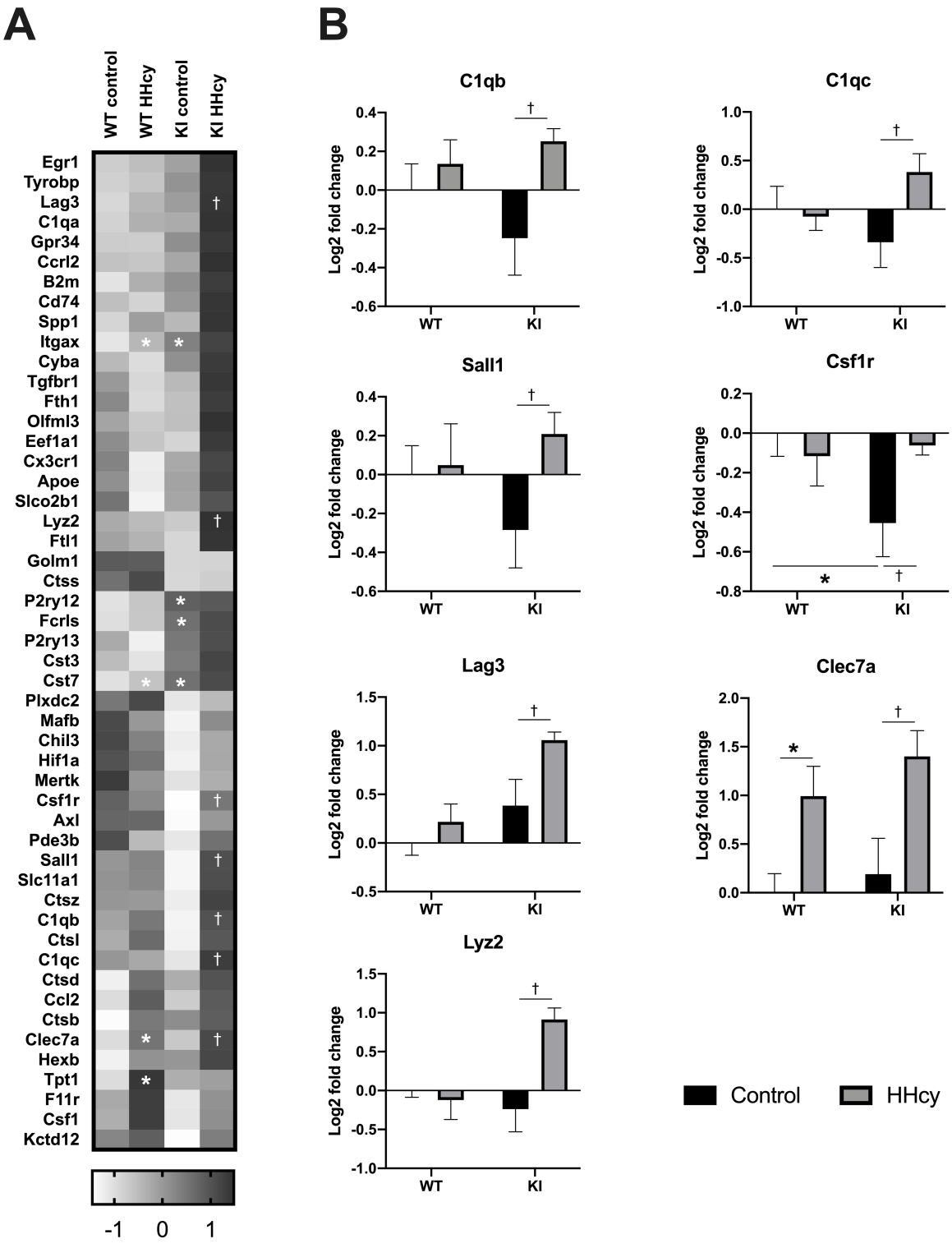

Figure 6

Microglial gene expression is altered in response to 8 weeks of HHcy diet in both WT and KI mice. A heatmap summarizing z-score transformed means of each gene across the 4 groups is displayed in (A). Individual graphs displaying log2 fold change values of 7 genes differentially expressed between KI control and KI HHcy mice are shown in (B). *p< 0.05 versus WT control, †p < .05 versus KI control, multiple t-tests, uncorrected.